Synthesis of carbon monoliths with a tailored hierarchical pore structure for selective CO_2 capture

D. Zabiegaj[a], M. Caccia[b], M. E. Casco[b], F. Ravera[a], J. Narciso[b,*]

[a]*CNR - Institute of Condensed Matter Chemistry and Technologies for Energy (ICMATE), via De Marini 6, 16149 Genoa, Italy.*
[b] *Instituto Universitario de Materiales de Alicante (IUMA), Universidad de Alicante, Apdo. 99, 03080 Alicante, Spain.*
**Corresponding author: narciso@ua.es*

ABSTRACT: Carbon monolithic adsorbents exhibiting a hierarchical pore structure are produced via a synthesis route based on the stabilization of liquid foams followed by a carbonization step. The macro-microporous structure is achieved by the incorporation of microporous, biomass-derived activated carbon particles in the liquid foam enclosed by a cationic surfactant as stabilizer. This method yields crack-free monoliths (solid foams) with a compressive strength of the order of 20 kPa. The microstructure and the textural properties of the final solid foams have been investigated by means of Scanning Electron Microscopy (SEM) and gas adsorption. The behavior as selective CO_2 adsorbents at 25 ºC has been evaluated using breakthrough experiments under simulated post-combustion conditions (16 % V/V CO_2/N_2), resulting in a selectivity factor of 13 over N_2. The hierarchical pore structure of the monoliths allows a rapid transport of the gas mixture through the macropores with no appreciable pressure drop, retaining more than 90% of the adsorption capacity (~ 0.868 mmol/g) after several adsorption/desorption cycles. Moreover, the monolith has shown a CO_2 uptake capacity of 2.62 mmol/g under static condition at 1 bar and 25 ºC. This study provides guidelines for the design of carbon-based foams decorated with carbon particles, which have morphological and textural properties that can be carefully selected for any gas-selective capture application.

1. Introduction

A concern for the emissions rise of greenhouse gases and their possible influence on global warming has led to an increase in research interest in several technologies with the capability of reducing the emissions of such gases or even removing them from the atmosphere. Of all greenhouse gases, the gas making the largest contribution from human activities is carbon dioxide (CO_2). Because of this, a significant amount of interest has been developed for the capture and the elimination of CO_2 from the atmosphere [1]. Post-combustion CO_2 capture at coal-powered power plants can be considered one of the most attractive short-term solutions to decrease CO_2 emissions, as the gaseous waste from these

power plants has been found to account for up to 25% of the annual CO_2 released globally [1]. The state-of-the-art technology used for CO_2 sequestration involves aqueous amine solutions which chemically adsorb CO_2 [2,3]. Unfortunately, this technology results in an energy penalty of around 20-30% of the output of the power plant required to regenerate the absorption unit [4]. Moreover, there is an environmental issue related to the corrosive nature of the amine solutions.

Novel systems based on adsorption phenomena have been investigated to overcome these drawbacks. For instance, a pressure or vacuum swing adsorption (PSA/VSA) unit is a promising technology that consists of a column filled with a properly designed adsorbent material, through which the gas stream flows, selectively capturing the CO_2 until the adsorbent reaches saturation. The subsequent regeneration is achieved by applying a change in pressure, resulting in a much cleaner and more cost-effective technology than the aforementioned aqueous amine solutions. In this procedure, the performance of the adsorption unit is governed by: the adsorption capacity of the material; the selectivity for the desired compound; the mechanical and chemical stability of the material, especially in the presence of moisture; and its capability to be regenerated. There are a great number of candidates among adsorbents to be used for this process such as zeolites [5,6], mesoporous silica [7-9], metal organic frameworks (MOFs) [10-12], porous organic polymers [13] and activated carbon [14-17]. The latter has proven to be a low-cost alternative with highly tunable features, such as high surface area, high thermal and chemical stability [18-21]. Furthermore, the current challenges in PSA/VSA based carbon capture are to significantly increase the productivity while ensuring high purity (95 %) and recovery (90 %) requirements. For instance, the selectivity in respect to other gases in the stream flow has to be very high. But at the same time, the CO_2-surface interaction has to be sufficiently weak to assure a fast regeneration of the carbon bed (i.e. high curvature of the CO_2 isotherm is detrimental) [22]. The largest disadvantage of activated carbon is that high-surface area carbon powder would produce a significant pressure drop in the gas stream if applied in columns [23]. Only a few previous attempts to produce high-surface area activated carbon monoliths have resulted in mechanically stable monoliths. For instance, Hao et al. [24] reported a carbon monolith prepared through a self-assembly of poly(benzoxazine-co-resol) followed by a carbonization process, which withstood a compressive stress of up to 15.6 MPa. A few years later, Hao et al. [25] reported a new type of hierarchically porous carbon monolith made from graphene oxide and asparagine

which was able to withstand up to 28.9 MPa. Recently, Fernandez-Catalá et al. [26] reported the preparation of AC@MOF hybrids using a binderless activated carbon monolith from petroleum residue with a crushing strength of *ca.* 8N. In any case, the mechanical resistance of the obtained monolith decreases with increasing surface area.

It is important to note that, in the area of ceramics, numerous techniques have been developed for the production of macroporous systems, the most common being reactive infiltration [27-30]. This technique has not been adapted to the manufacture of carbon foams, however it has been successfully applied to the synthesis of metallic foams [31]. In recent years, a new method, based on the solidification of particle-stabilized liquid foams, was developed for ceramic foams [32,33]. This approach has been successfully adapted to the production of macroporous carbon foams, using carbonaceous particulates, such as carbon black or carbon soot [34, 35] as foam stabilizer. The carbon porous materials obtained exhibited a highly ordered macroporous system with a cell structure interconnected by struts. According to the method proposed in these studies, liquid foams stabilized by carbon colloidal particles are used as a template for a gel-casting process. The polymeric porous material obtained, also called "green body", is further treated at high temperature to eliminate the organic components and obtain porous carbon materials. A key aspect of this method is that the formulation of the initial liquid foam determines the structural and mechanical features of the final porous materials. By associating surfactant to solid nanoparticles it is possible to tune their degree of hydrophobicity, which consequently affects their affinity with the water-air interface and, therefore its effectiveness as foam stabilizer. Thus, the physico-chemical characterization of the precursor dispersions by determining the interfacial and bulk properties, is a fundamental step to monitor and select the right degree of the particle amphiphilicity. For example, it has been shown that after associating appropriate surfactants to carbon particles in the dispersion, it is possible to improve the mechanical strength and increase the specific surface area of the final porous materials.

In the present work, we apply this technique by using *ad hoc* produced microporous activated carbon powders as stabilizers of the precursor liquid foams. By using microporous particles, we obtained mechanically stable carbon monoliths with hierarchical micro/macro pore structures. The textural and structural properties of the monoliths were evaluated and the performance of the monoliths for CO_2 adsorption under both static and dynamic conditions were tested.

2. Experimental

2.1 Materials

Activated carbon particles were produced in-house from milled coconut shell through a physical activation process using CO_2 as activating agent [35,36]. Two particle size fractions were selected through sieving for this purpose, a fine fraction (20-50 μm) and a coarse fraction (50-100 μm). After sieving, the milled coconut shell was washed using a 1 M HCl solution and rinsed with distilled water. Both fractions were carbonized at 800 ºC for 1 hour with a heating rate of 1 ºC/min. Afterwards, the obtained carbon particles were activated using CO_2 at 950 ºC for 6 hours with a heating rate of 10 ºC/min. The obtained activated carbon particles were characterized using gas adsorption (N_2 and CO_2) and scanning electron microscopy (SEM).

The cationic surfactant used to stabilize the liquid foams, hexadecyltrimethylammonium-bromide (CTAB); the gel-casting agents, Polyvinyl alcohol (PVA), the cross-linker 2,5-dimethoxy-2,5-dihydrofuran (DHF) and Nitric acid (HNO_3), were supplied by Sigma-Aldrich (Germany). The water employed for the preparation of the dispersions was obtained by using a multi-cartridge system (Millipore, Elix plus Milli-Q), providing a resistivity greater than 18 MΩ·m and surface tension of 72.5 mN/m without any appreciable kinetics over several hours.

2.2 Procedure

2.2.1 Carbon particles and carbon monoliths characterization

The textural properties of the activated carbon particles and the carbon monoliths produced were evaluated using physical adsorption (N_2 adsorption at -196 ºC and CO_2 adsorption at 0 ºC). Measurements were performed up to 1 bar in an in-house-built, fully-automated manometric equipment designed and constructed by the Advanced Materials Group, now commercialized as N2Gsorb-6 (Gas to Materials Technologies; www.g2mtech.com). Before any adsorption measurements, samples were degassed at 250 ºC for 4 hours. The surface area was calculated using the Brunaeur-Emmet-Teller theory applied to the N_2 adsorption data (S_{BET}). The narrow micropore volume ($V_{DR,CO2}$) and the micropore volume ($V_{DR,N2}$) were calculated by applying the Dubinin-Radushkevich equation to the CO_2 and N_2 adsorption isotherms, respectively. Adsorption measurements were performed using

whole monolithic specimens. The structure of the monoliths was evaluated using scanning electron microscopy (SEM) and field emission scanning electron microscopy (FESEM).

2.2.2 Particle dispersion preparation

Activated carbon particles dispersions were prepared by stepwise addition of the aqueous phase (CTAB solution) upon continuous stirring. To ensure full dispersion of the particles, suspensions were put under sonication for 1 hour and they were kept under stirring overnight. Afterwards, a 3.9 wt.% PVA solution was added gradually to the mixture. To avoid particle agglomeration, dispersions were stirred overnight.

2.2.3 Interfacial and bulk characterization of particle dispersions

The surface tension of the dispersions, γ, was measured by the drop shape tensiometry technique [38]. This method is based on the acquisition of the drop/bubble shape under gravity effect. The surface tension is determined by fitting the theoretical profile of an axis-symmetric drop calculated through the Laplace equation to each experimentally acquired drop profile. The instrument used in this work (PAT-1, Sinterface, Germany) allows the surface tension versus time, with an accuracy of 0.1 mN/m, to be measured using a pendant drop formed at the tip of a small Teflon capillary of a few millimeters in diameter. The instrument allowed the drop/bubble surface area during the surface tension measurement to be automatically controlled by means of a precision syringe pump. In this study, the drop surface area was maintained at a constant value of 30 mm^2 while the surface tension was acquired over time until the achievement of the equilibrium value. All the measurements were performed at 25 ºC.

The size distribution and the surface charge of the AC particles in the water dispersions were obtained by Dynamic Light Scattering (DLS) and zeta-potential measurements, respectively, using a Zetasizer device (Nano ZS, Malvern Instruments, United Kingdom). In DLS measurements, the intensity correlation function of the dispersions was obtained using the red line (λ = 632 nm) of a He-Ne laser at a fixed temperature of 25 ºC and a quasi-backscattering configuration (θ = 173°). The hydrodynamic diameter dH is obtained by the analysis of the normalized second order correlation functions g2(t) using a standard inverse Laplace algorithm which provides the apparent diffusion coefficient, D, related to the particles size through the Stokes-Einstein relation. The zeta-potential was calculated from measurements of electrophoretic mobility (μe) obtained by laser Doppler

electrophoresis technique [39]. All measurements were performed in disposable capillary cells at a fixed controlled temperature of 25 ºC.

2.2.4 Porous monolith preparation

The solid foams, or porous monoliths, were prepared according to the procedure written elsewhere [34,35]. The liquid foams are generated from the previously prepared and homogenized dispersions, using a direct foaming technique. With this purpose, a special mixer (T25 ULTRA-TURRAX, IKA) beats the dispersion for 2-10 minutes, with a speed of 8,000-10,000 rpm. In order to obtain the green body foam, immediately after foaming, the particle-laden foams are placed into the oven for 4 hours at 80 ºC, where they undergo solidification by *in situ* gelation. The prepared materials were cooled to room temperature and left to dry for 48 hours. The whole procedure is summarized in Fig 1.

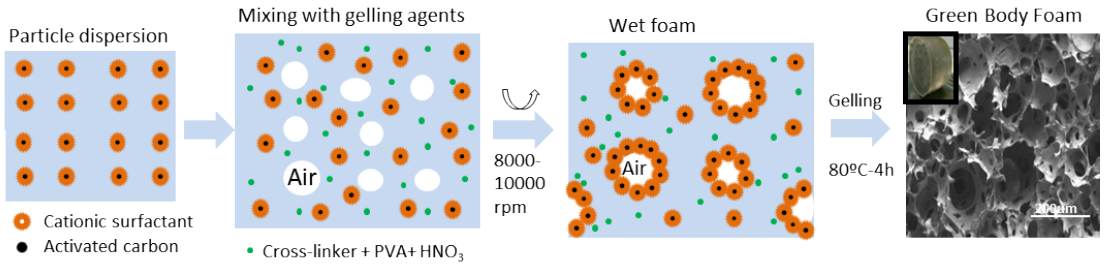

Fig 1. Schematic representation of the green foam synthesis procedure.

After drying, green foams were carbonized at 900 ºC for 1 hour using a heating rate of 1 ºC/min under argon flow to obtain the carbon monoliths. For comparison, a monolith using only PVA binder without AC particles was produced following the same procedure.

2.2.5 Gas adsorption capacity

The single component CO_2 and N_2 adsorption capacities were measured at 25 ºC up to 1 bar in an in-house-designed, fully-automated manometric equipment designed and constructed by the Advanced Materials Group, now commercialized as N2Gsorb-6 (Gas to Materials Technologies; www.g2mtech.com). Adsorption measurements were performed using whole monolithic specimens.

The separation measurements of CO_2 from CO_2/N_2 binary mixture were performed in a fixed-bed column (inner diameter of 3.2 mm and a length of 60 mm containing *ca.* 100 mg of sample) at 25 ºC and a total pressure of 1 bar. Prior to the experiment, the adsorbent was

cleaned at 200 ºC for 2 hours under a He flow of 50 mL/min. The breakthrough experiment was carried out by switching abruptly from a He flow of 40 mL/min to the mixture gas containing 16 % of CO_2 (V/V) in N_2 with a total flow of 10 mL/min. The flow rates of all gases were controlled by a mass flow controller with an accuracy of ±0.1 mL/min. The temperature was measured using a thermocouple with an accuracy of ±1 ºC located immediately outside the column at the solid bed. The temperature was monitored during the experiment. The evolution of the effluent gas was monitored in a mass spectrometer (Pfeiffer, OmniStar GSD 301). Six cycles of adsorption/desorption were performed to evaluate the selectivity and reversibility of the monolith under milder regeneration condition. After each breakthrough run the regeneration was carried out by switching the feed gas back to a pure He flow of 40 mL/min at 25 ºC for 20 minutes. The same experiment in an empty column was performed in order to obtain a correction factor which represented the time required for the gases to flow from the saturator valve to the detector in the absence of adsorption phenomena.

The dynamic adsorption capacity (q) of the adsorbents was calculated from the breakthrough curves at break time according to the equation [14, 40]:

$$q = \frac{F}{m}\left(\int\left(1-\frac{C}{C_0}\right)\cdot dt - t_D\right)$$

where F is the molar flow of gas, m is the amount of the adsorbent in the fixed bed, C and C_0 are the outlet and inlet concentration of the stream through the system, respectively, and t_D is in the dead volume of the system.

3. Results and discussion

3.1 Activated carbon particles characterization

The N_2 and CO_2 isotherms obtained at -196 and 0 ºC respectively (Fig 2) for the fine and coarse activated carbon particles produced showed that there seemed to be no effect of the particle size in the development of porosity during activation. Both particle sizes present a N_2 type I isotherm with a very narrow knee, indicating the presence of narrow micropores. Both activated carbons show high CO_2 adsorption capacity of around 4.8 mmol/g at 0 ºC. The pore size distribution calculated using the NLDFT model (slit-shaped pore; equilibrium model) confirms the presence of narrow microporosity with pore diameters below 1 nm. SEM analysis (Fig. 2) shows that the particles present random geometries,

retaining biological features of the precursor used (coconut shell). The surface area calculated from N_2 isotherms using the BET method was 900 m^2/g, and the narrow micropore volume and micropore volume calculated from the N_2 and CO_2 isotherms using the Dubinin-Radushkevich method are, 0.35 and 0.39 cm^3/g respectively, for both particle sizes.

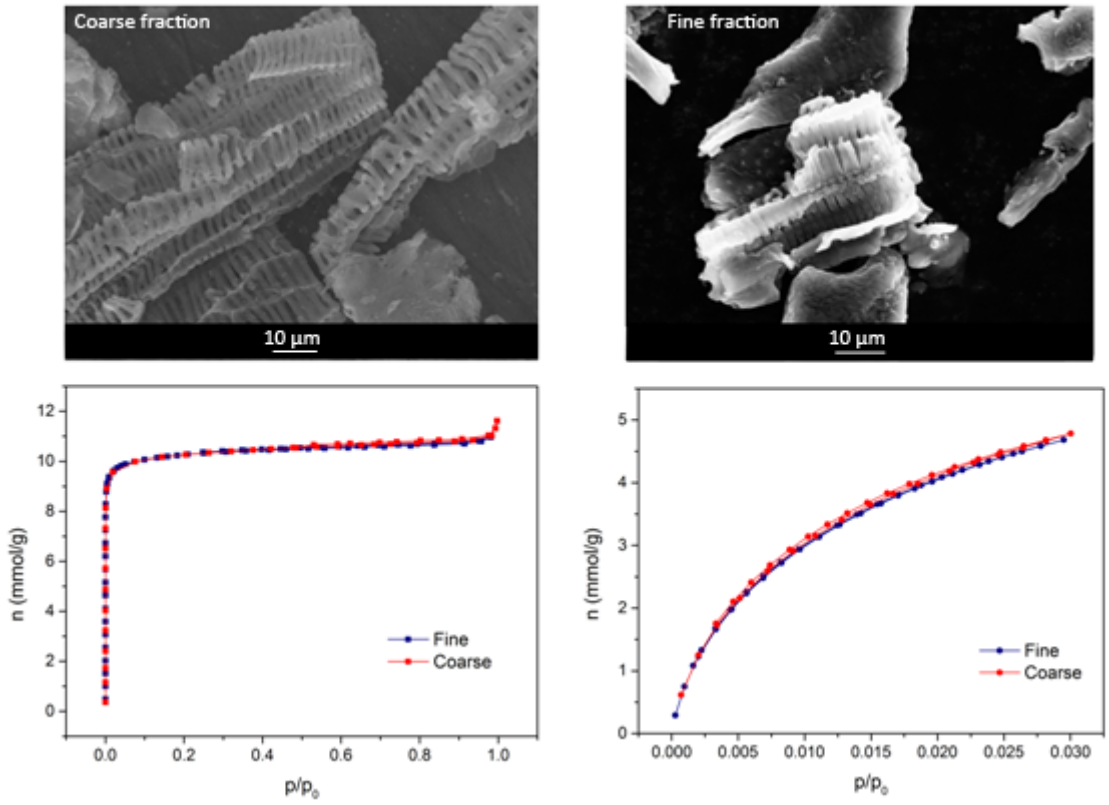

Fig 2. SEM representative images of the as-produced activated carbon particles and gas adsorption measurements (N_2 and CO_2 isotherms obtained at -196 ºC and 0 ºC respectively).

3.2 Dispersion characterization

The activated carbon (AC) particles investigated presented a very low capacity to be dispersed in pure water while stable dispersions were obtained in the presence of CTAB surfactant, even at low concentration. This allowed the characterization of the dispersions from both the point of view of the surface properties, by means of surface tension measurement, and with regards to the bulk characteristics of surfactant modified AC particles. In pure water, carbon particles tend to aggregate and precipitate. Improvement of the dispersion in the CTAB solution as compared to the water solution could be explained

by the surfactant molecules adsorbing onto the AC carbon surface, driven by hydrophobic interactions, thereby creating a new hydrophilic surface layer which is more compatible with the water matrix. As already discussed in [41] for a similar system, the adsorption of CTAB limited the particle aggregation. Moreover, AC–CTAB complexes present an amphiphilic character and tend to transfer to the water-air interfaces, which can stabilize foams. In fact, a common way to control foam formation and stability is to mix the particles with an oppositely charged ionic surfactant. Tuning the surfactant adsorption on solid particles allows the degree of hydrophobicity to be controlled, improving in some cases also the dispersion stability [42].

In order to find the appropriate formulation of the liquid, the mixed AC-CTAB dispersions were characterized by means of surface tension and zeta-potential measurements as a function of the CTAB concentration (Fig 3). Figure 3a shows the equilibrium surface tension of a dispersion of 0.1 wt.% AC particles in an aqueous CTAB solution vs. CTAB concentration (blue points) compared with the values obtained for the corresponding CTAB solution without particles (black points). The black line is the best-fit curve obtained from the Frumkin adsorption isotherm. Fig. 3b shows the zeta-potential values obtained for the same dispersions vs. the surfactant concentration.

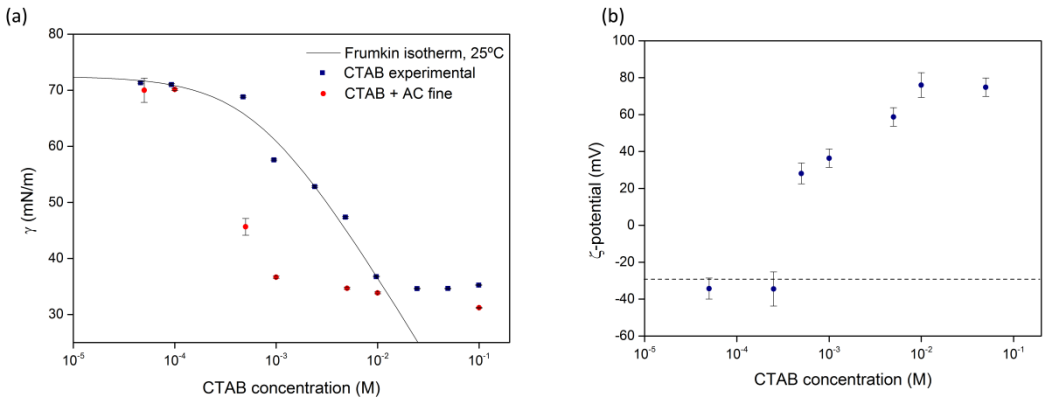

Fig 3. (a)Equilibrium surface tension of the AC-CTAB dispersion (blue points), of the CTAB solution (black points) and best fit theoretical curve by the Frumkin adsorption isotherm; (b) zeta-potential of the AC-CTAB dispersion. The dashed line indicates the zeta-potential of distilled water.

At low CTAB concentrations, $< 5 \cdot 10^{-5}$ M, the surface tension of the AC-CTAB dispersions and of the corresponding CTAB solution are similar. This changes dramatically for CTAB concentrations around $5 \cdot 10^{-4}$ M and higher, where the surface tension of the AC-CTAB

dispersion decreases abruptly to about 45 mN/m. For CTAB concentrations higher than $1 \cdot 10^{-3}$ M, the equilibrium surface tension of the dispersion presents a nearly constant value. This behavior can be compared with the data obtained by the zeta-potential measurements. As reported in Figure 3b, when increasing the surfactant concentration, the initially negative charge of particles (-20 mV) is neutralized and, for CTAB concentration higher than $5 \cdot 10^{-4}$ M, it becomes positive. Around this charge inversion point, we can assume that CTAB-decorated particles are partially hydrophobic and tend to be transferred to the water-air interface. This is consistent with the significant surface tension decrease observed for CTAB concentration around $5 \cdot 10^{-4}$ M. Further increase of surfactant concentration provokes the growth of the positive particle charge, due to the increase of CTAB adsorption onto the particle surface. When the complexes assume a rather high positive charge, that is for CTAB concentration of around $1 \cdot 10^{-3}$ M and higher, the particles are expected to become hydrophilic and remain in aqueous phase rather than on the interface. This is in agreement with the surface tension measurements. This analysis of the surface and bulk properties of the AC-CTAB dispersions provides the optimum surfactant concentration in which particles are transferred to the water-air interface becoming efficient foam stabilizers. From these results, we can assume that the optimum ratio between particles and surfactant corresponds to a CTAB concentration of $4 \cdot 10^{-4}$ M in an AC dispersion of 0.1 wt.%. That means that the dispersion should present an AC/CTAB ratio of 2.5 g/mmol to optimize the transfer of particles to the water/air interfaces in the liquid foams. No effect of particle size was evidenced in the dispersion behavior for the particle size fractions used in this work. For the sake of clarity, only the measurements corresponding to the fine fraction are shown.

3.3 Green monolith characterization

Several green body foams were prepared according to the procedure described in the previous section using activated carbon particles of both sizes. The initial solid content of particles in dispersions was 1 and 10 wt.%. The concentration of CTAB was chosen in order to maintain the optimum AC/CTAB ratio of 2.5 g/mmol. After *in situ* gelation, the materials obtained present a crack-free monolithic aspect, retaining the shape of the container used for their production, allowing for the production of custom geometries. As evidenced by SEM analyses (Fig 4), the skeleton of the obtained monoliths consists of large and medium homogeneously interconnected spherical cells.

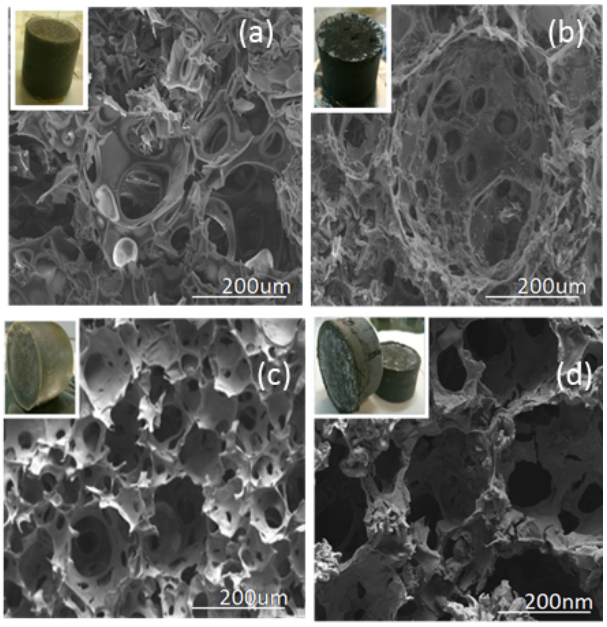

Fig 4. SEM images of (a) green body foams of 1 wt.% coarse AC particles , (b) 10 wt.% of coarse AC particles, (c) 1 wt.% fine AC particles and (d) 10 wt.% fine AC particles.

The open cell structure is mainly an effect of the surfactant presence in the matrix foam. For comparison, the corresponding samples of green body carbon foam without surfactant were prepared. The resulting foams are more compact and present a structure dominated by heterogeneous closed cells (see Fig 5a and b). Furthermore, a closer look at the cell walls of green foams prepared with surfactant revealed the presence of bumps and a certain topography which can be attributed to the AC particles that are covered in PVA during the gelling process (see Fig 5c). This provides further evidence of the segregation of particles to the air/liquid interface during foaming.

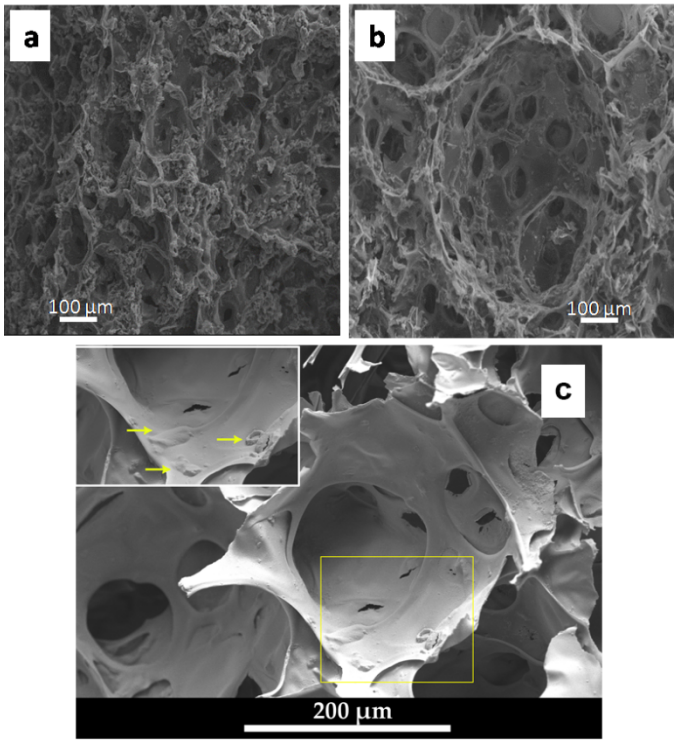

Fig 5. (a) SEM images of samples produced without surfactant and (b) with CTAB. (c) SEM image of a green body obtained with surfactant. Arrows indicate the presence of bumps in the foam cell wall.

3.4 Carbon monoliths characterization

After the carbonization step, monoliths experienced a volume decrease of around 60% but retained their geometry and no cracking was observed. Carbonized monoliths were robust enough to withstand handling and machining operations (cutting and drilling). The compressive strength of these monoliths is of the order of ~ 20 kPa as reported by Zabiegaj et al. [41,42] for similar materials. SEM observations indicate that they also retained the cell structure of the green foams. Interestingly, the observed bumps in green foams disappeared after the heat treatment, and were replaced by AC particles embedded in the wall of the cells (see Fig 6).

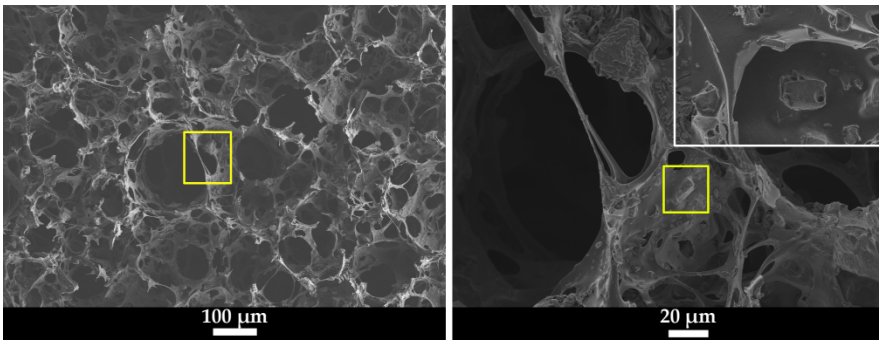

Fig 6. SEM image the carbon monoliths produced, where the embedded AC particles in the walls of the cells are evidenced. The areas marked in yellow have been magnified for better observation.

Fig 7 shows the N_2 isotherms at -196 ºC and the CO_2 isotherms at 0 ºC obtained for the different carbon monoliths, including that of the green foam and the carbon monolith synthesized in absence of AC particles (only PVA). The green foam presented a type III N_2 isotherm, characteristic of non-porous materials, probably because the AC particles are covered by PVA. However, all carbonized monoliths, including the PVA foam, showed type I N_2 isotherms, indicating the presence of microporosity. In Table 1 the B.E.T. surface area, the narrow micropore volume (pores diameters below 0.7 nm) and micropore volume (pores diameters below 2 nm) for all the samples are presented. The samples containing 10 wt.% AC particles show the highest B.E.T. surface areas, which are slightly inferior to the one of the AC powder. The narrow micropore volume ($V_{DR,CO2}$) is similar in all of the carbon monoliths, ranging from 0.31-0.37 cm^3/g. The micropore volume ($V_{DR,N2}$) ranges from 0.24-0.25 cm^3/g for monoliths containing 1 wt.% AC and 0.30-0.32 cm^3/g, for monoliths containing 10 wt.% The fact that the $V_{DR,CO2}$ is higher that the $V_{DR,N2}$ is an indication that the pore size distribution is tight in the narrow pore diameter range (below 0.7 nm), which means that these materials are promising for the capture and separation of small gas molecules, like CO_2. However, since the pore size is so small, larger molecules, like N_2, cannot diffuse into the inner porosity and are, therefore, not isolated. Moreover, the carbonization of PVA also yields a microporous material ($V_{DR,CO2}$ = 0.24 cm^3/g), indicating that the final textural properties of the carbon monoliths is a combination of the remaining accessible pores of the AC particles and the newly developed narrow micropores in the carbonized PVA phase.

Table 1**.** Textural properties derived from gas adsorption measurements of the produced monoliths.

Sample	Particle size fraction	AC content in the initial dispersion (wt %)	S_{BET} (m^2/g)	$V_{DR,N2}$* (cm^3/g)	$V_{DR,CO2}$*(cm^3/g)
AC	Coarse/Fine	-	900	0.36	0.39
Carbon monolith	Coarse	1	630	0.24	0.32
Carbon monolith	Coarse	10	800	0.30	0.32
Carbon monolith	Fine	1	630	0.25	0.31
Carbon monolith	Fine	10	850	0.32	0.37
PVA monolith	-	0	140	0.06	0.24
Green foam	Coarse	10	16	0.11	0.11

$V_{DR,CO2}$, $V_{DR,N2}$= narrow micropore volume and micropore volume calculated by applying Dubinin-Radushkevich to the CO_2 and N_2 adsorption isotherm data, respectively.

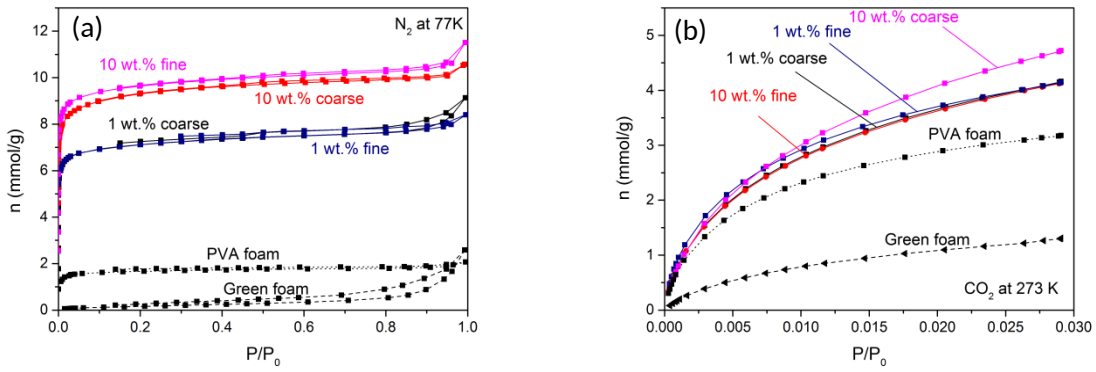

Fig. 7.(a) N_2 isotherms obtained at -196 ºC and (b) CO_2 isotherms obtained at 0 ºC for the different monoliths produced. The solid lines correspond to AC-containing monolithic samples, and the dashed and dotted line corresponds to the green foam and the PVA foam respectively.

The micropore size distribution of the different monoliths was calculated using the NLDFT model applied to the CO_2 adsorption isotherm data (slit-shaped pore; equilibrium model), and the results are shown in Fig. 8. These calculations confirm that the microporosity developed in the carbonized PVA phase is narrower than the microporosity of AC particles. AC particles also exhibit two small peaks at the pore sizes around 0.75 and 0.85 nm (dashed lines) that are also present in the AC-containing monoliths, thus indicating an excellent interconnection between the micropores in the particles and the macropores of

the monolith. This hierarchical macro-micro pore structure guarantees a rapid transport of the gas through the macropores of the monoliths into the narrowest micropores (pores below 0.7 nm) of the AC particles where CO_2 will be adsorbed, suggesting that the monoliths produced using this technique can be excellent adsorbent materials for selective CO_2 capture in CO_2/N_2 streams in a gravimetric basis.

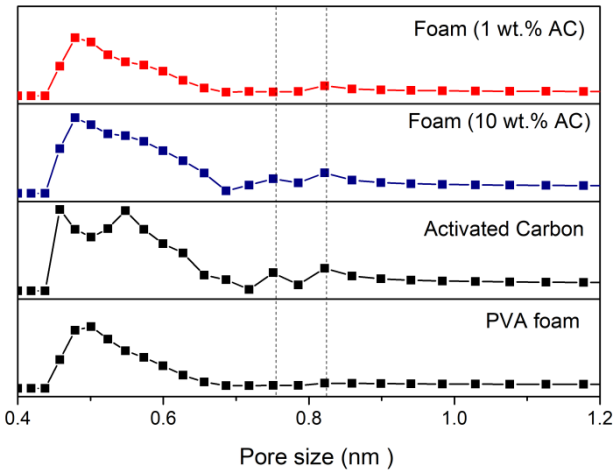

Fig. 8. Micropore size distribution (PSD_{micro}) obtained using the NLDFT model.

The macropores were shown to exhibit geometries similar to spheres and consist of a net of cells interconnected by struts of smaller diameter. The macropore size distribution was evaluated using mercury porosimetry (see Fig. 9), and the results indicate a narrow pore size distribution around the average pore size, as observed qualitatively in SEM previously. There is not a very distinctive effect of particle size or content on the resulting macropore size distribution of the monoliths; however, it seems that higher content in AC particles yields slightly larger macropores. Nevertheless, it must be taken into account that the pore sizes measured using mercury porosimetry only represent the size of the pore entrance and that the actual pore might be larger. A more realistic pore size can be derived from SEM observations.

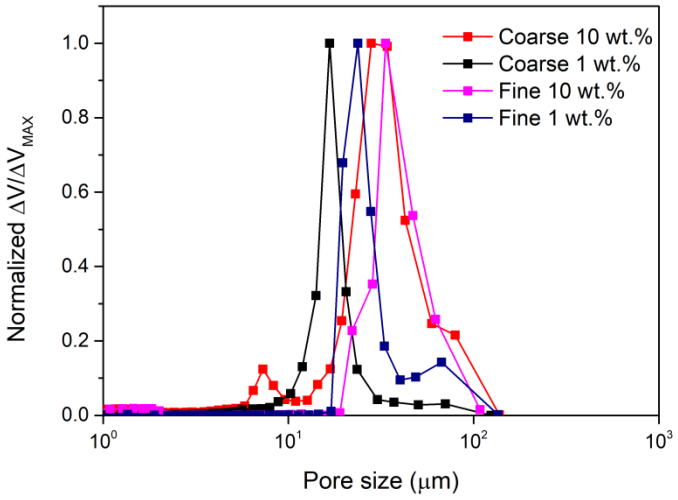

Fig. 9. Macropore size distribution (PSD_{macro}) obtained using mercury porosimetry.

3.5 CO_2 selective capture from CO_2/N_2 mixtures

In order to evaluate the potential of CO_2 capture technologies, the sample with 10 wt.% fine AC was selected and placed into a column for further breakthrough experiments under a simulated post-combustion exhaust stream of a coal-powered power plant. The sample monolith was machined from a larger monolith using the same quartz reactor employed for the adsorption experiment as a drill, thus ensuring that there were no gaps between the sample and the walls of the reactor. Fig. 10a shows the results obtained from a fixed-bed column system with an inner diameter of 3.2 mm and a length of 60 mm containing 0.082 mg of sample. A feed gas mixture composed of 16% (V/V) of CO_2 in N_2 was used and the experiment was carried out at 25 ºC at a total pressure of 1 bar. The measured dynamic CO_2 adsorption capacity was 0.868 mmol/g, which is slightly smaller than the static adsorption capacity of the single component at the same relative pressure of 0.16 bar (0.992 mmol/g, see Fig. 11). This difference is expected since the isotherm is built up point by point in the volumetric equipment waiting for the thermal equilibrium in the sample cell at each pressure. Moreover, the isotherms are obtained using a single gas component, while in the breakthrough experiment there is competition for the adsorption sites between CO_2 and N_2. Facing practical application, the working capacity of the column (the CO_2 uptake) is a critical factor to make the PSA process more efficient. Indeed, the fact that the working capacity of the sample under the dynamic experimental conditions is very close to the maximum adsorption capacity under equilibrium conditions is due to the hierarchical pore structure that allows a fast transport of the gas through the macropores of the monolith to

the micropores of the activated carbon allocated in the walls of the monolith resulting in a small mass transfer zone (i.e. enhanced column efficiency) as anticipated by looking at the vertical profile of the breakthrough curve [20].

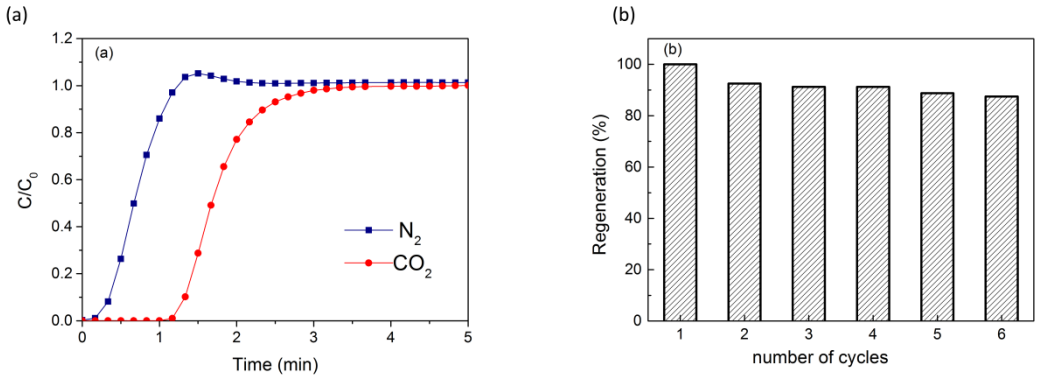

Fig. 10. (a)Breakthrough curve of a 10 wt.% AC carbon monolith using a CO_2 (16%)/N_2 (84%) flue gas mixture at 25 ºC and atmospheric pressure. (b) Regeneration of the same specimen throughout six cycles of adsorption/desorption run.

Moreover, the selectivity factor ($S_{CO2/N2}$) was calculated as:

$$S_{CO_2/N_2} = \frac{q_{CO_2}/y_{CO_2}}{q_{N_2}/y_{N_2}}$$

where q_{CO2} and q_{N2} are the equilibrium dynamic adsorption amounts of CO_2 and N_2 at the breakthrough time respectively. y_{CO2} and y_{N2} are the mole fraction of CO_2 and N_2 in the gas phase. The CO_2 selectivity over N_2 gives a value of ca. 13, superior to that exhibited for a commercial Norit type activated carbon calculated from the adsorption of the single component [42] and well-within the range of selectivities reported for several adsorbents [11,14,21,27]. Several cycles of adsorption-desorption were performed in order to test the stability and recyclability of the carbon monolith under milder regeneration conditions (a He flow of 40 mL/min for 20 minutes at 25 ºC). Fig. 10b shows that the sample retains more than 90% of its initial capacity after six consecutive cycles. The easy regeneration is in accordance to the low enthalpy of adsorption of CO_2 on the carbon surface 22 kJ/mol [14]. Works from Casco et al [15] and Presser at al. [43] nicely described systematically the effect of the pore size on carbon dioxide sorption by carbon materials. Note that the maximal CO_2 adsorption capacity of the carbon foam with 10% of fine AC under static condition is 2.62 mmol/g at 1 bar/25 ºC and 4.13mmol/g at 1 bar/0ºC. Although these

values are not the highest value reported in the literature for carbon-based adsorbent [44], they follow the trend found for carbon materials containing similar micropore volume and pore size below 0.7 nm of the above-cited articles, and are comparable to others microporous adsorbents, such as metal organic frameworks [11] or microporous organics polymers [17,45].

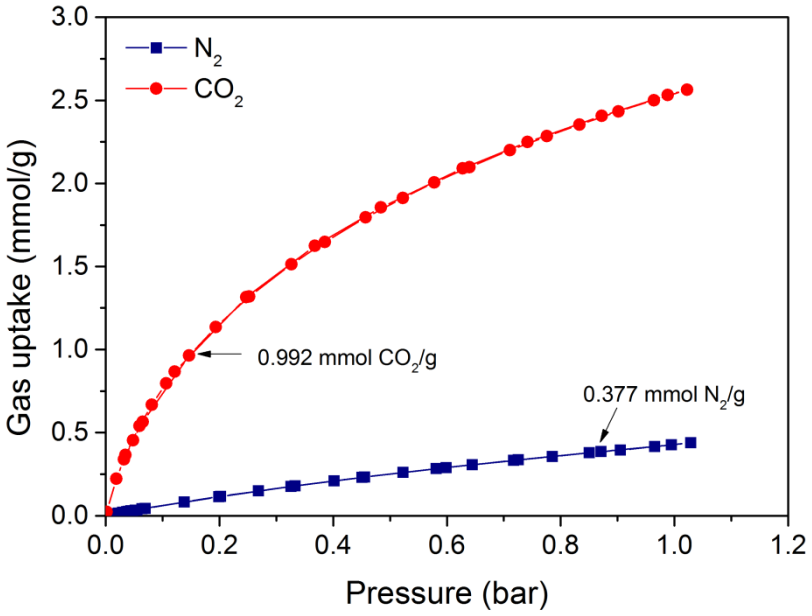

Fig. 11. Equilibrium adsorption isotherms of the single component CO_2 and N_2 at 25 ºC up to 1 bar for a 10 wt.% AC monolith.

In summary, this synthesis method can yield hierarchical carbon monoliths able to adsorb considerable amounts of CO_2 in both static and dynamic conditions at very low relative pressure (0.16 bar) and at ambient temperature, combining high stability and recyclability after several runs. The shape of the monolith can be tailored in order to facilitate handling in the industry toward PSA carbon capture technologies and its adsorption capabilities can be tuned by modifying the constituent particles used.

4. Conclusions

Carbon porous materials were obtained by adapting a previously-developed method based on the combination of direct foaming and gel-casting. According to this method, liquid foams stabilized by solid particles are used as templates for the synthesis of macroporous materials. We used *ad hoc* produced activated carbon powders with important micro-porosity, obtaining carbon monoliths with a hierarchical porosity. As indicated by surface

tension measurements of the precursor dispersions, such activated carbon particles interacting with cationic surfactants, become amphiphilic and tend to segregate to the air/liquid interface, guaranteeing the foaming and the high stability of the obtained liquid foams. The monoliths produced here show excellent gravimetric CO_2 adsorption capacities and proved to have a good performance in the selective CO_2 capture under simulated post combustion gas streams. The interconnected macro and micropore network guarantees a rapid transport and adsorption of CO_2 with no observable pressure drop along the column. Furthermore, the samples showed to retain their working capacity even upon cycling. By changing the morphology or/and textural properties of the carbon particles, it is possible to design a great variety of hierarchical porous materials. For instance, it could be possible to extend the protocol to other carbon colloids such as carbon nanotubes or graphene.

Acknowledgements

The authors would like to acknowledge the financial support received from Generalitat Valenciana (PROMETEO II/2014/004-FEDER and PhD grant Vali+d), the University of Alicante (Ayudas para estancias de personal investigador invitado) and the Italian Space Agency, ASI, within the Project PASTA "Particle Stabilized Emulsion and Foams" (n. 2013-028-R.O).

References

1. IPCC (2005) IPCC special report on carbon dioxide capture and storage. Working Group III of the Intergovernmental Panel on Climate Change. Metz B. et al. (eds). Cambridge University Press, New York, NY, USA, 442.
2. G.T. Rochelle, Amine scrubbing for CO_2 capture, Science, **325** (2009) 1652-4.
3. www.globalccsinstitute.com/projects
4. IPCC (2007) Climate change 2007: mitigation. Contribution of Working Group III to the Fourth Assessment Report of the Intergovernmental Panel on Climate Change. Metz B, et al (eds). Cambridge University Press, New York, NY, USA.
5. J. Hennessy, CO2 capture: Bespoke zeolites, Nature Materials, **14** (2015), 857.
6. R. V. Siriwardane, M. Shen, E. P. Fisher, Adsorption of CO_2 on zeolites at moderate temperatures, Energy Fuels, **19** (2005) 1153–1159.
7. C. H. Yu, C. H. Huang, C.S. Tan, A review of CO_2 capture by absorption and adsorption, Aerosol and Air Quality Research, **12** (2012) 745-769.

8. N. Gargiulo, F. Pepe, D. Caputo, Modeling carbon dioxide adsorption on polyethylenimine-functionalized TUD-1 mesoporous silica, Journal of Colloid and Interface Science. **367** (2012) 348-354.
9. F. Brandani, D. Ruthven, The Effect of Water on the Adsorption of CO_2 and C3H8 on Type X Zeolites, Industrial & Engineering Chemistry Research, **43** (2004) 8339–8344.
10. A.R. Millward, O.M. Yaghi, Metal organic frameworks with exceptionally high capacity for Storage of carbon dioxide at room temperature, Journal of the American Chemical Society, **127** (2005) 17998-17999.
11. V. Safarifard et al., Influence of the Amide Groups in the CO_2/N_2 Selectivity of a Series of Isoreticular, Interpenetrated Metal–Organic Frameworks, Crystal Growth & Design.**16**(2016), 6016−6023.
12. N. C. Burtch, H.Jasuja, K. S. Walton, Water stability and adsorption in metal–organic frameworks, Chemical reviews, **114** (2014) 10575-10612.
13. L. Zou et al., Porous Organic Polymers for Post-Combustion Carbon Capture, Advanced Materials, **29** (2017) 1700229.
14. M.G. Plaza, S. García, F. Rubiera, J.J.Pis, C. Pevida, Post-combustion CO_2 capture with a commercial activated carbon: Comparison of different regeneration strategies, Chemical Engineering Journal **163** (2010) 41–47.
15. M.E. Casco, M. Martínez-Escandell, J. Silvestre-Albero, F. Rodríguez-Reinoso, Effect of the porous structure in carbon materials for CO_2 capture at atmospheric and high-pressure, Carbon, **67** (2014) 230-235.
16. M. E. Casco et al., CO_2 adsorption on crystalline graphitic nanostructures, Journal of CO_2 Utilization, **5** (2014) 60–65.
17. A. Rehman, S. Park, Facile synthesis of nitrogen-enriched microporous carbons derived from imine and benzimidazole-linked polymeric framework for efficient CO_2 adsorption, Journal of CO_2Utilization, **21** (2017) 503–512.
18. T. C. Drage, J. M. Blackman, C.Pevida, C. E. Snape, Evaluation of activated carbon adsorbents for CO_2 capture in gasification, Energy Fuels, **23** (2009), 2790–2796.

19. N. A. Rashidi, S. Yusup, A. Borhan. Isotherm and thermodynamic analysis of carbon dioxide on activated carbon, Procedia Engineering, **148** (2016) 630-637.
20. H. Marsh, F. Rodríguez-Reinoso, Activated Carbon. Elsevier, 2006.
21. N.A. Rashidi, S. Yusup, An overview of activated carbons utilization for the post-combustion carbon dioxide capture, Journal of CO_2 Utilization, **13** (2016) 1-16.
22. M. Khurana, S. Farooq, Integrated adsorbent-process optimization for carbon capture and concentration using vacuum swing adsorption cycles, AIChE, **63** (2017)2987-2995.
23. B. Crittenden et al., Carbon monoliths: A comparison with granular materials, adsorption, **11** (2005) 537–541.
24. G.P. Hao, et al., Structurally designed synthesis of mechanically stable poly(benzoxazine-co-resol)-based porous carbon monoliths and their application as high-Performance CO_2capture sorbents, Journal of the American Chemical Society, **133** (2013) 11378–11388.
25. G.P Hao, et al., Porous carbon nanosheets with precisely tunable thickness and selective CO_2 adsorption properties, Energy& Environmental Science, **6** (2013) 3740.
26. J. Fernández-Catalá, M.E. Casco, M. Martínez-Escandell, F. Rodríguez-Reinoso, J. Silvestre-Albero, HKUST-1@ACM hybrids for adsorption applications: a systematic study of the synthesis conditions, Microporous and Mesoporous Materials, **237** (2017) 74e81.
27. M. Caccia, J. Narciso, Production of SiC materials by reactive infiltration, Materials Science Forum, **783** (2014) 1863-1866.
28. M. Caccia, et al., Towards optimization of SiC/$CoSi_2$ composite material manufacture via reactive infiltration: Wetting study of Si–Co alloys on carbon materials, Journal of the European Ceramic Society, **35** (2015), 4099-4106.
29. N.R. Calderón, M. Martínez-Escandell, J. Narciso, F. Rodríguez-Reinoso, The combined effect of porosity and reactivity of the carbon preforms on the properties of SiC produced by reactive infiltration with liquid Si, Carbon, **47** (2009) 2200-2210.
30. N.R. Calderón, M. Martínez-Escandell, J. Narciso, F. Rodríguez-Reinoso, The role of carbon biotemplate density in mechanical properties of biomorphic SiC, Journal of the European Ceramic Society, **29** (2009) 465-472.

31. H. Salavagione, R. Prieto, E. Morallón, J. Narciso, 3D Electrodes from aluminium foams prepared by replication process, Journal of Applied Electrochemistry, **40** (2010) 241-246.
32. J. R. Jones, L. L. Hench, Current Opinion in Solid State and Materials Science, **7**(2003) 301-307.
33. P. Sepulveda, J. G. P. Binner, Processing of cellular ceramics by foaming and in situ polymerization of organic monomers, Journal of the European Ceramic Society, **19** (1999) 2059-2066.
34. D. Zabiegaj, E. Santini, E. Guzman, M. Ferrari, L. Liggeri, V. Buscaglia, M. T. Buscaglia, F. Ravera, Nanoparticle laden interfacial layers and application to foams and solid foams, Colloids and surfaces A, **438** (2013) 132-140.
35. D. Zabiegaj, E. Santini, M. Ferrari, L. Liggeri, F. Ravera, Carbon based porous materials from particle stabilized wet foams, Colloids and Surfaces A, **473** (2015) 24–31.
36. F. Rodríguez-Reinoso, M. Molina-Sabio, M.T. Gonzalez, The use of steam and CO_2 as activating agents in the preparation of activated carbons, Carbon, **33** (1995), 15-23.
37. F. Rodríguez-Reinoso, M. Molina-Sabio, Activated carbons from lignocellulosic materials by chemical and/or physical activation: an overview, Carbon, **30** (1992), 1111-1118.
38. G. Loglio, P. Pandolfini, L. Liggieri, A. K. Makievski, F. Ravera, Determination of interfacial properties by the pendant drop tensiometry-optimisation of experimental and calculation procedures, in: R. Miller and L. Liggieri (Eds.), Bubble and Drops Interface, Brill, Leiden-The Netherlands, 2011, 7–38.
39. Smith, B. R. Ware, Apparatus and methods for laser doppler electrophoresis, in: D. M. Hercules, G. M. Hieftje, L. R. Snyder and M. A. Evenson (eds.). Contemporary topics in analytical and clinical chemistry, Berlin-Heidelberg, Sprinter, 1978, 29–54.
40. M.S.Shafeeyan, W. Mohd, A.W. Daud, A. Shamiri, N. Aghamohammadi, Modeling of carbon dioxide adsorption onto ammonia-modified activated carbon: kinetic analysis and breakthrough behavior, EnergyFuels, **29** (2015) 6565-6577.
41. D. Zabiegaj, M.T.Buscaglia, D. Giuranno, L. Liggieri, F. Ravera, Activated carbon monoliths from particle stabilized foams, Microporous and Mesoporous Materials, **235** (2027), 45-53.

42. D. Zabiegaj, E. Santini, E. Guzman, M. Ferrari, L. Liggeri, F. Ravera, Carbon soot–ionic surfactant mixed layers at water/air interfaces, Journal of Nanoscience and Nanotechnology, **15** (2025), 3618.
43. V. Presser, J. McDonough, S. Yeon, Y. Gogotsi, Effect of pore size on carbon dioxide sorption by carbide derived carbon, Energy & Environmental Science, **4** (2011) 3059.
44. A.E. Creamer, B. Gao, Carbon-Based Adsorbents for Post-combustion CO_2 capture: a critical review, Environmental Science & Technology, **50** (2016) 7276-7289.
45. Y. Xu, D. Chang, S. Feng, C. Zhang, J. Jiang, BODIPY-containing porous organic polymers for gas adsorption, New Journal of Chemistry, **40** (2016) 9415.